Supplementary information

Constructing Ru–porphyrin COF for catalyzing air oxidation of adamantane C–H bonds to relay olefin epoxidation

Dongpo Li [a,1], Qianqian Mao [a,1], Chao Xiong [a,*], Luying Xi [a], Yu Nie [a], Xiaotian Xu [a], Hongbing Ji [a,*]

[a] State Key Laboratory of Green Chemical Synthesis and Conversion, Institute of Green Petroleum Processing and Light Hydrocarbon Conversion, College of Chemical Engineering, Zhejiang University of Technology, Hangzhou, 310014, China.

[1] These authors contributed equally to the paper

*Corresponding Authors:

*Xiong Chao: xiongclh@zjut.edu.cn;

*Hongbing Ji: jihb@ zjut.edu.cn;

1. Experiments

1.1 Characterizations

The crystal structure patterns and the atomic states of the catalysts were recorded by an X-ray powder diffractometer (RIGAKU, D/max 2200v, Japan) with a diffraction angle 2θ range of 5−80° at a scanning speed of 10°/min. Infrared spectra were recorded using a Thermo Fisher Scientific NICOLET 6700 FT-IR spectrometer with the spectral range of 400−4000 cm^{-1}. The N_2 adsorption-desorption isotherms and thermal stability of the catalyst were recorded by a Micromeritics ASAP 2020 plus BET adsorption analyzer and a Netzsch TG209F1 libra TG-MS analyzer under an air atmosphere, respectively. The ^{13}C solid state nuclear magnetic resonance spectra of the catalyst were measured by using a Bruker Advance III 500 nuclear magnetic resonance spectrometer. A Nexsa X-ray photoelectron spectroscopy (XPS) was used to explore the composition and valence states of the catalyst. SEM images of the catalyst were collected by a field-emission Gemini 500 scanning electron microscope (Bruker, Germany) with an energy-diffusive X-ray spectroscopy (EDS) attachment. The high-resolution transmission electron microscopy (HR-TEM) images of the samples were obtained by JEM-2100 Plus (LaB6 filament) at 300 kV. The *in-situ* IR spectra was recorded by a Mettler Toledo ReactIR iC10 *in-situ* IR spectrometer. The free radical signals of the catalytic system in this were obtained by a EPR 200-Plus Electron paramagnetic resonance Spectrometer (ESR, CIQTEK Co., Ltd., China), and the adducts between the trapping agents and the free radicals in 1-butene epoxidation were detected by a Thermo MAT95XP HRMS spectrometer. Moreover, the reaction substrates and products were quantified via a Shimadzu gas chromatography (GC, GC2014plus, Japan) with a flame ionization detector and a capillary column (Rtx-5, 30 m × 0.32 mm × 0.25 μm). And a Shimadzu gas chromatography mass (GCMS-QP2010, Japan) spectrometry was used to identify the reaction products.

1.2 Catalyst Preparation

The amorphous Ru-porphyrin polymer (Ru-POF-TPD) was synthesized following the reported literature methods [1,2]. Typically, pyrrole (134 mg, 2.0 mmol) and 4,4'-biphenyldicarboxaldehyde (210 mg, 1.0 mmol) were added to a round-bottom flask containing 200 mL of acetic acid. Subsequently, 4-nitrobenzaldehyde (5 mL) and trifluoroacetic acid (1 mL) were added sequentially under stirring. The resulting mixture was stirred continuously at 80 °C for 12 h, then cooled to room temperature. The crude product was filtered, washed with deionized water for three times, and further rinsed with 100 mL of ethanol. After vacuum drying at 80 °C for 24 h, a black powder was obtained. Then, a 50 mg portion of this black powder was uniformly dispersed in 50 mL of decahydronaphthalene, and 20 mg of $Ru_3(CO)_{12}$ was added to the suspension. The mixture was stirred continuously at 180 °C for 12 h and then cooled to room temperature. The resulting Ru-POF-TPD was isolated by filtration, washed successively with 20 mL of ethanol (three times) and 20 mL of deionized water (three times), and finally dried under vacuum at 80 °C overnight (Scheme S1). Meanwhile, XRD analysis revealed that it exhibited only a single broad diffraction peak at 22° (Figure S2).

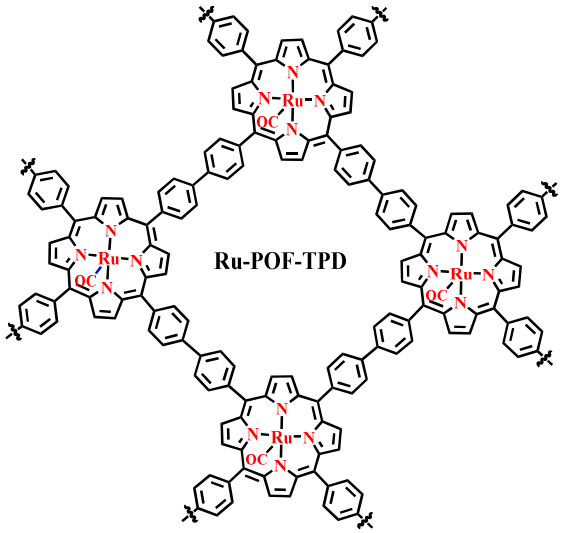

Scheme S1. The structure of Ru-POF-TPD.

In the synthesis of Ru-COF-TPA, Ru-COF-TPF and Ru-COF-TPQ, the same procedure as that for Ru-COF-TPD were followed, except that 1,4-phthalaldehyde (26.8 mg, 0.2 mmol), 4,4"-p-terphenyldicarboxaldehyde (57.2 mg, 0.2 mmol) and

[1,1':4',1":4",1"'-quaterphenyl]-4,4"'-dicarbaldehyde (72.4 mg, 0.2 mmol) were used as raw materials.

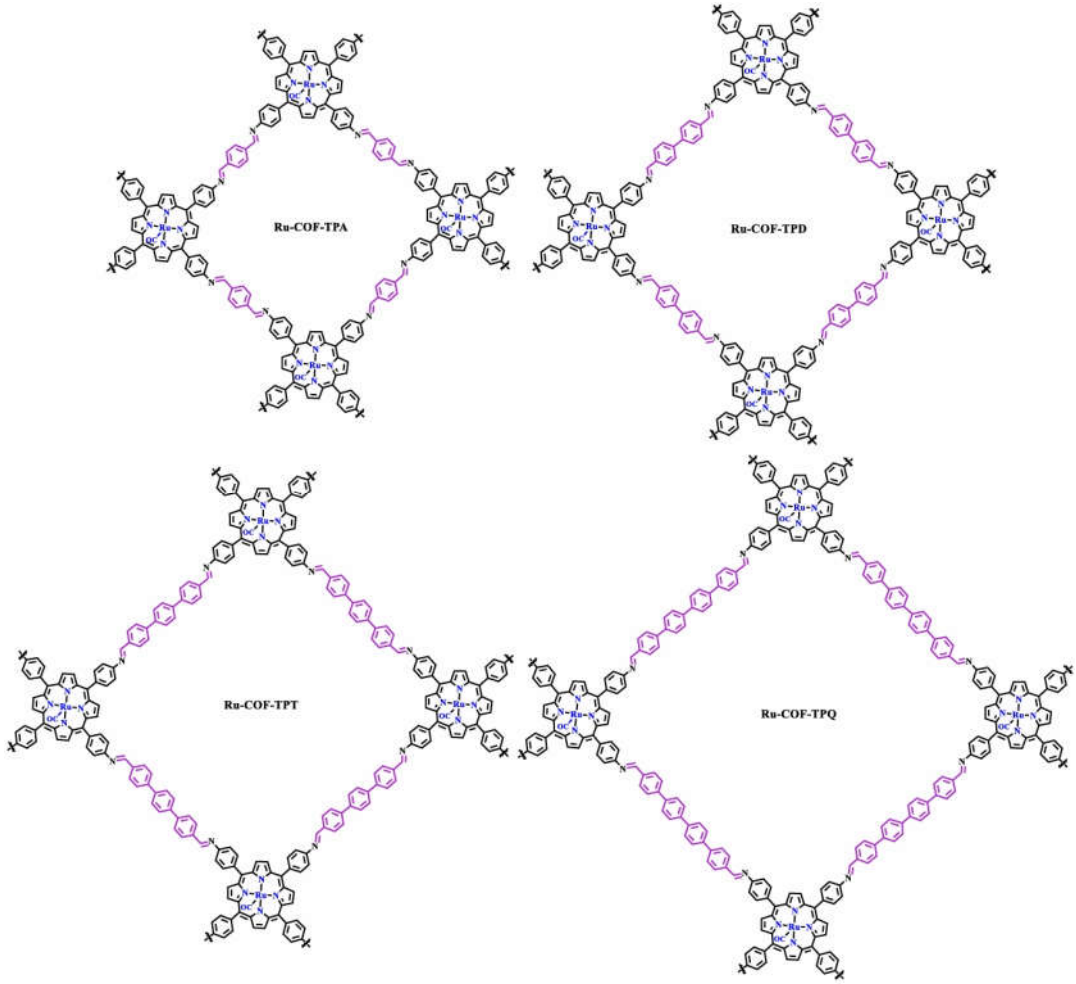

Scheme S2. Synthesis of Ru-COFs with different linkers.

The Ru-COF-1 was synthesized following the reported literature methods [1,2]. As shown in Scheme S3, typically, 134.8 mg TPP-NH_2 (0.2 mmol), 84.0 mg PDD (0.4 mmol), 20 mL solvent (*o*-DCB/n-butanol=1/1) and 1 mL HOAc were added to a 50 mL Schlenk tube under the N_2 atmosphere, respectively. Subsequently, the resulting solution was then stirred continuously at 120 °C for 72 h. Subsequently, the crude product was filtered, washed with deionized water for three times, and further rinsed with 100 mL of ethanol. After vacuum drying at 80 °C for 24 h, a black powder was obtained. Then, the black solid powder obtained above was uniformly dispersed in 50 mL of decahydronaphthalene, and 46 mg of $Ru_2(CO)_6Cl_4$ (0.09) was added to the suspension. The mixture was stirred continuously at 180 °C for 12 h and

then cooled to room temperature. The resulting Ru-COF-1 was isolated by filtration, washed successively with 20 mL of ethanol (three times) and 20 mL of deionized water (three times), and finally dried under vacuum at 80 °C overnight. In the synthesis of Ru-COF-2, the same procedure as that for Ru-COF-1 was followed, except that RuO_2 (23.9 mg, 0.18 mmol), was used as raw material.

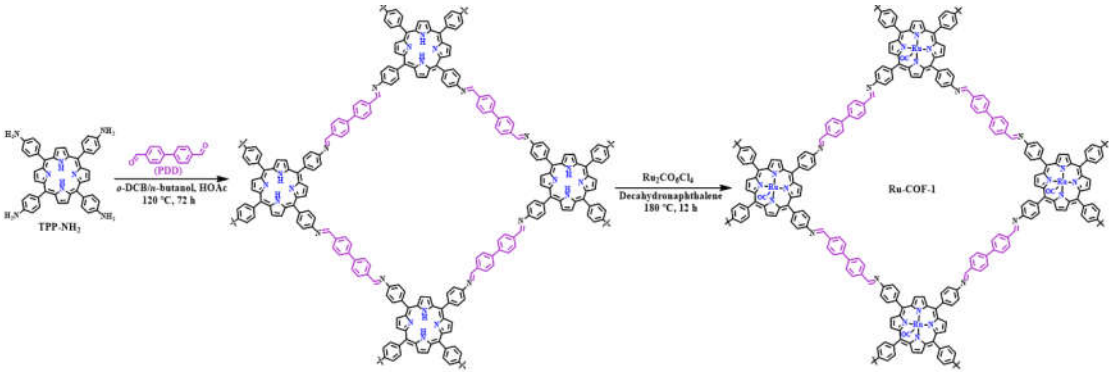

Scheme S3. Synthesis of Ru-COF-1.

1.3 Thermodynamics analysis

The macroscopic thermodynamic fitting curves for the formation of the corresponding product from 1-butylene over Ru-COF-TPD were fitted using the Van't Hoff equation (Eq. S1). The entropy change (ΔS^{θ}, $J \cdot K^{-1} \cdot mol^{-1}$) and enthalpy change ($\Delta H^{\theta}$, $J \cdot mol^{-1}$) were calculated using Eq. S2. K_d (mL/mg) represents the equilibrium constant and was calculated using Eq. S3. Q denotes the conversion amount of 1-butylene and was calculated using Eq. S4.

$$\ln(K_d) = \frac{-\Delta G^{\theta}}{RT} \tag{S1}$$

$$\Delta G^{\theta} = \Delta H^{\theta} - T \cdot \Delta S^{\theta} \tag{S2}$$

$$K_d = \frac{Q}{C^{f}_{(HE)}} \tag{S3}$$

$$Q = \frac{(C^{i}_{(HE)} - C^{f}_{(HE)}) \times V_{(sys)}}{M_{(catal.)}} \tag{S4}$$

Where, T, R, and ΔG^{θ} were, respectively, the absolute temperature in Kelvin, the universal gas constant (8.314 $J \cdot mol^{-1} \cdot K^{-1}$), and Gibbs free energy change (J/mol).

And $C^{i}_{(HE)}$, $C^{f}_{(HE)}$, $V_{(sys)}$, and $M_{(catal.)}$ were the initial concentration of 1-butylene, the final concentration of 1-butylene, the volume of the reaction system, and the mass of catalyst, respectively.

1.4 Kinetics analysis

Epoxidation kinetic curves of 1-butylene over Ru-COF-TPD were fitted by using three common semiempirical models (zero-order, pseudo-first-order, and pseudo-second-order), and the apparent activation energy (Ea) of the oxidation reaction was calculated by the Arrhenius equation.

$$Linear\ Zero\ order: C_o - C_t = k_o t + C \tag{S5}$$

$$Linear\ pseudo-first\ order: \ln(Q_m - Q_t) = \ln(Q_1) - k_1 t \tag{S6}$$

$$Linear\ pseudo-second\ order: \frac{t}{Q_t} = \frac{1}{k_2 \cdot Q_2^{\ 2}} + \frac{t}{Q_2} \tag{S7}$$

$$Arrhenius\ equation: \ln k = \ln A - \frac{E_a}{RT} \tag{S8}$$

Where, C_0 and C_t (mg/mL) were the initial and time t (min) concentrations of 1-hexene, respectively. k_0, k_1 (min^{-1}), and k_2 ($g \cdot mg^{-1} \cdot min^{-1}$) were the kinetic rate constants of zero-order, pseudo-first-order, and pseudo-second-order, respectively. Q_m, Q_t, Q_1, and Q_2 (mg/mg) were then converted amounts of 1-butylene at equilibrium, the converted amounts of 1-butylene at time t (min), the equilibrium converted capacity of pseudo-first and the equilibrium converted capacity of pseudo-second order, respectively. Furthermore, A and k were the reaction rate constant and a pre-exponential factor of the Arrhenius equation, respectively.

1.5 RMSE calculations

The calculation of root means square error (RMSE) was shown in Eq. S9.

$$\sqrt{\frac{(x_1 - x_1')^2 + (x_2 - x_2')^2 + \cdots + (x_n - x_n')^2}{N}} \tag{S9}$$

Where, N, n, x_n and x_n' were, respectively, the sample size, experiment times, predicted, and true values. In this work, the RMSE values were calculated by a mathematical fitting software.

1.6 Control experiment

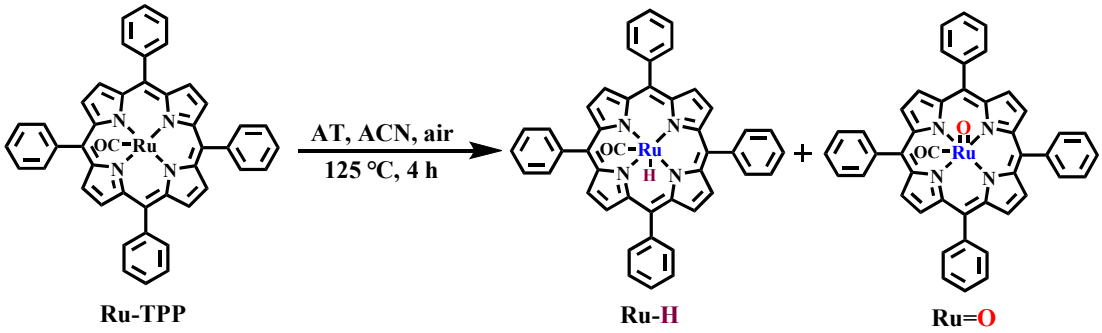

Reaction conditions: Ru-TPP (10 mg), adamantane (2.7 g, 20 mmol), ACN (20 mL) were added to the reactor with a magnetic bar. The reactor was then charged air at 2.5 MPa. Subsequently, it was transferred to an oil bath maintained at 125 °C for 6 h. The reaction products were analyzed via high-resolution mass spectrometry (HRMS).

1.7 The product distribution of adamantane under optimal conditions.

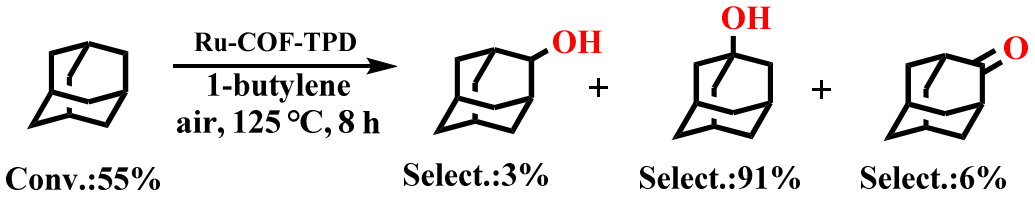

Under optimal conditions (8 mmol cyclohexene, 20 mmol adamantane, 10 mg Ru-COF-TPD, 20 mL acetonitrile, 2.5 Mpa air, 125 ℃, 8 h), the conversion rate of adamantane was 55%, the selectivity of the product 1-adamantanol was 91%.

1.8 Carbon balance calculation

Taking 1-butene as an example: the reaction was conducted under the optimal conditions. Upon the completion of the reaction, the reactor was cooled to room temperature, and the gaseous and liquid phases inside the reactor were collected

separately with precise volume quantification, which were then injected into a gas chromatograph (GC) using a calibrated microsyringe. The gaseous phase was analyzed by a thermal conductivity detector (TCD), whereas the liquid phase was detected with a flame ionization detector (FID). As shown in Figure S29, no over-oxidized gaseous products (e.g., CO_2 and CO) were detected in the gaseous components. Residual 1-butene was subsequently identified in the gaseous phase via FID detection, and the amount of 1-butene in the gaseous phase (n_1) was calculated based on the 1-butene calibration curve, injection volume and peak area from the GC chromatogram. Unreacted 1-butene was also detected in the liquid phase, and its content (n_2) was determined by the identical method. Finally, the consumed amount of 1-butene (n_3) was calculated from the 1-butene conversion. The sum of n_1, n_2 and n_3 should be equivalent to the initial amount of 1-butene charged into the reactor prior to the reaction. The calculated results gave n_1 = 0.03 mmol, n_2 = 1.45 mmol and n_3 = 6.48 mmol, leading to a theoretical amount of 1-butene of 7.96 mmol, which was approximately consistent with the actual initial charging amount (8 mmol).

2. Supporting Figures and Tables

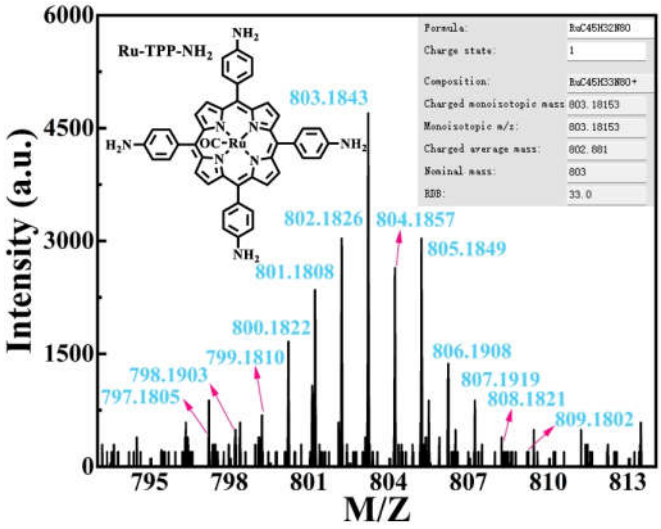

Figure S1. HRMS analysis of Ru-TPP-NH_2

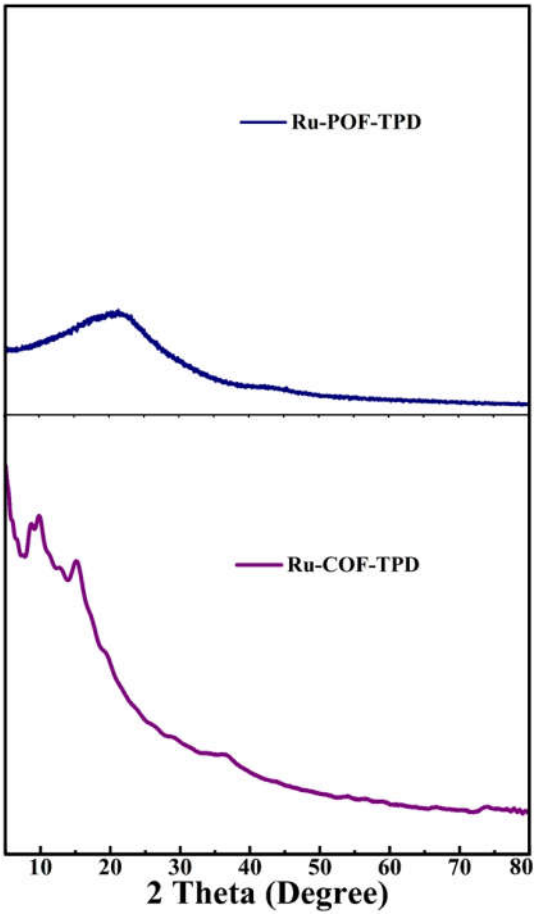

Figure S2. PXRD spectra of Ru-POF-TPD and Ru-COF-TPD.

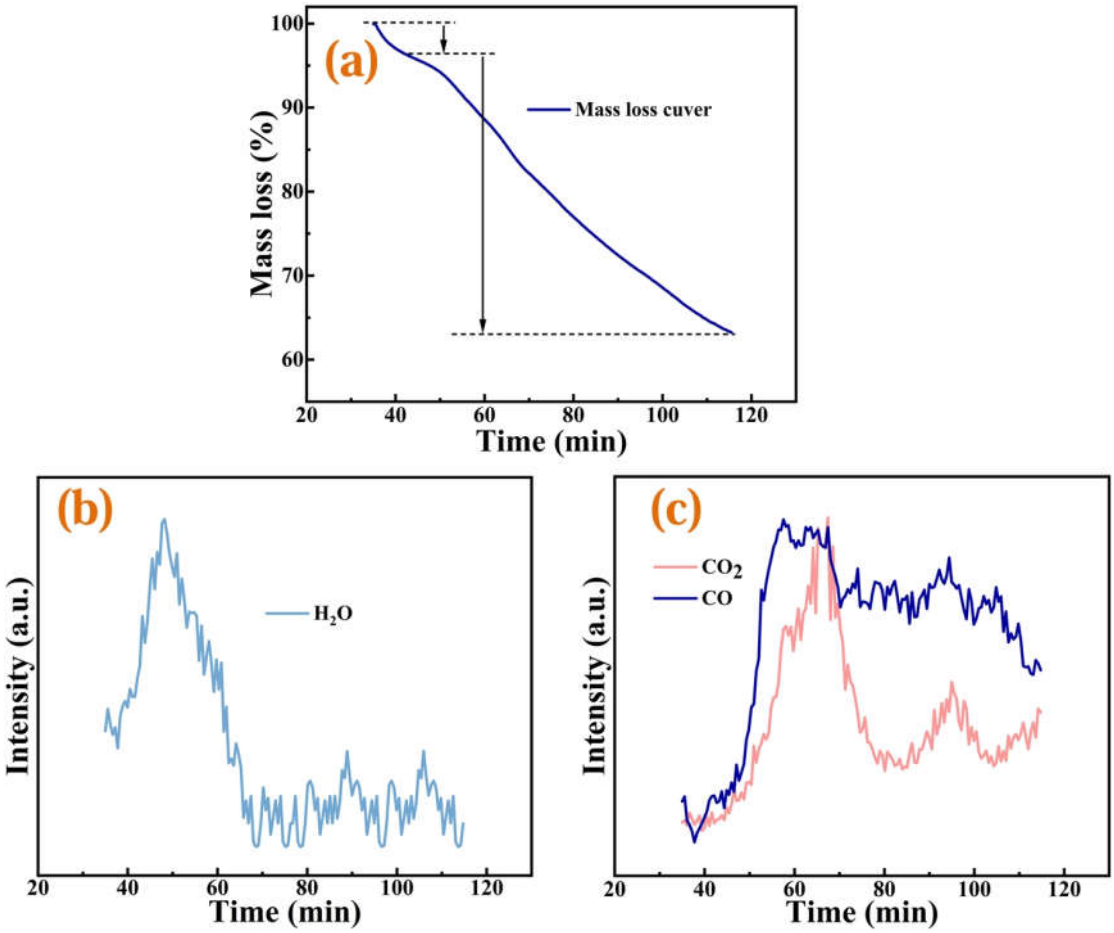

Figure S3. (a) TGA curve with time, (b) MS spectra of moisture content with time, and (c) MS spectra of CO and CO_2 with time.

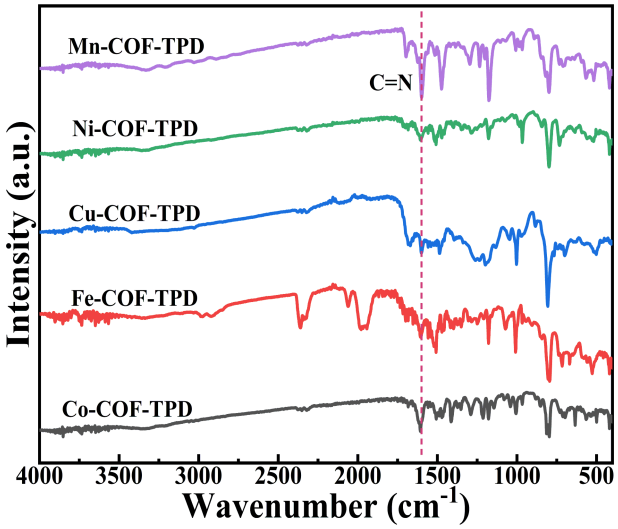

Figure S4. FT-IR spectra of Co-COF-TPD, Fe-COF-TPD, Cu-COF-TPD, Ni-COF-TPD and Mn-COF-TPD.

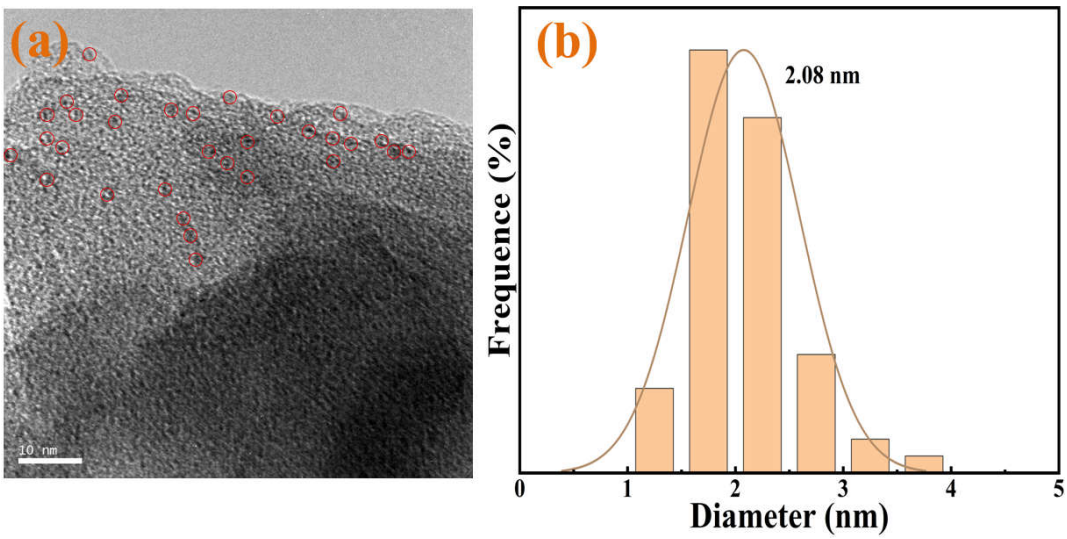

Figure S5. (a) TEM images for Ru-COF-TPD, (b) particle diameter spectra of Ru metal.

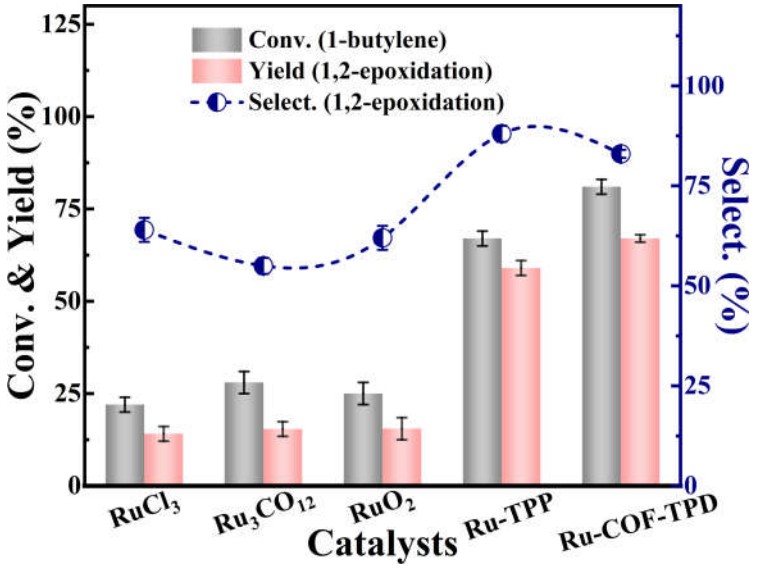

Figure S6. Comparison of the catalytic performance among $RuCl_3$, Ru_3CO_{12}, RuO_2, Ru-TPP and Ru-COF-TPD.

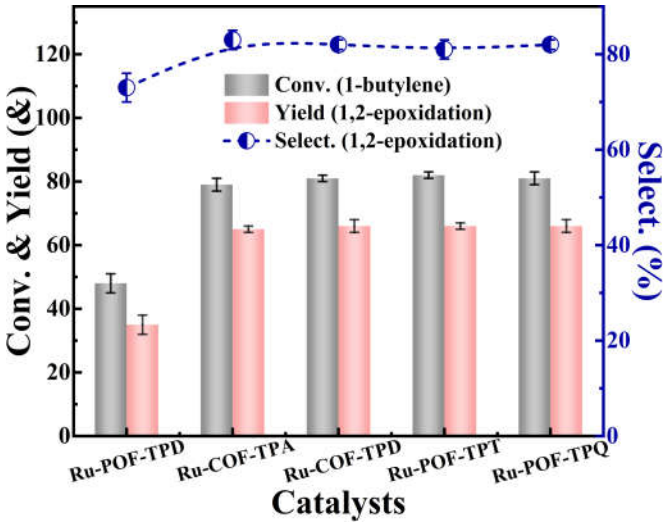

Figure S7. The catalytic performance of the different catalysts in 1-butylene epoxidation.

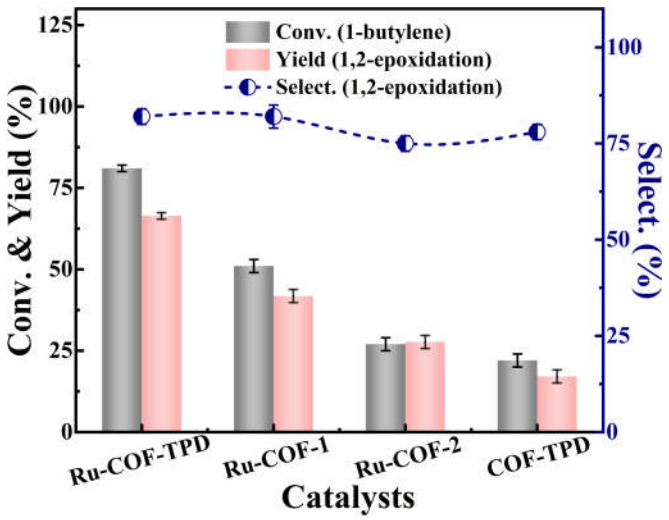

Figure S8. Comparison of the catalytic performance with different Ru precursors.

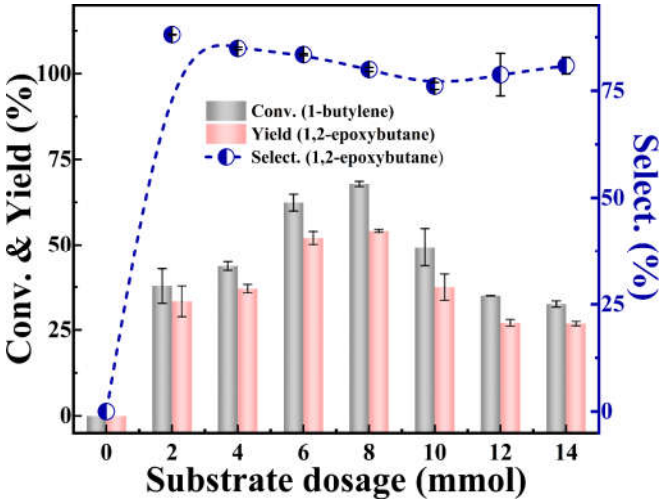

Figure S9. Effect of different substrate dosage on the epoxidation of 1-butylene.

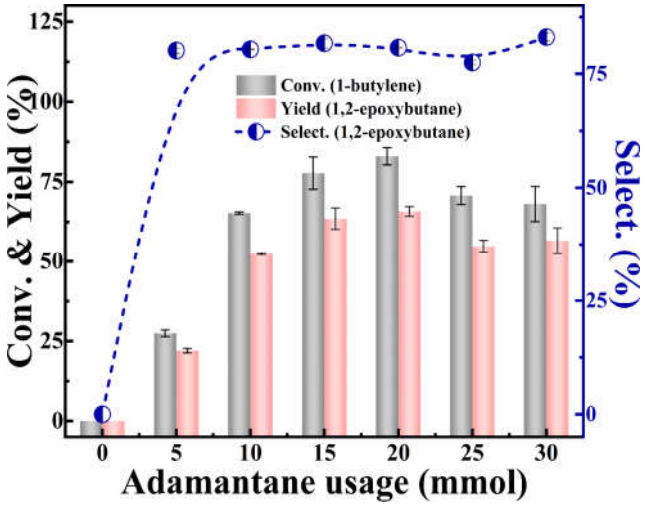

Figure S10. Effect of different adamantane usage on the epoxidation of 1-butylene.

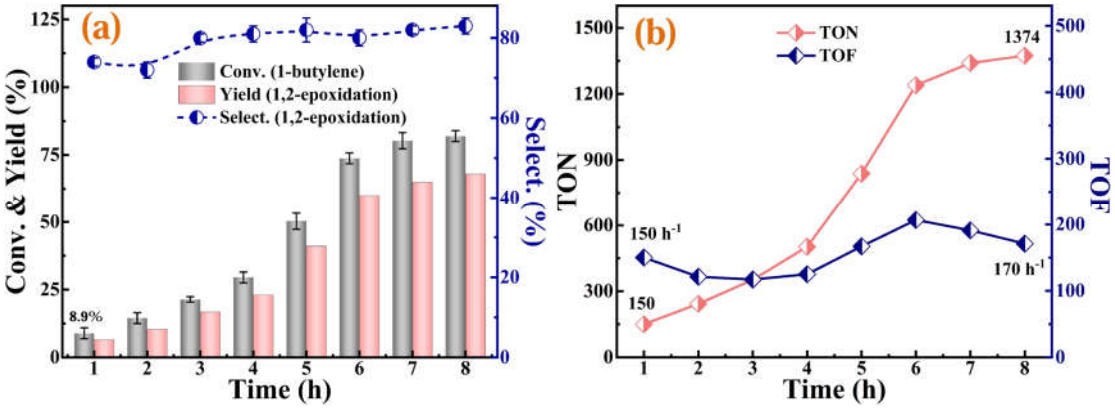

Figure S11. (a) Substrate conversion at different reaction times under optimal conditions with other parameters held constant, (b) the turnover number (TON) and turnover frequency (TOF) of Ru-COF-TPD at different reaction time. The calculation of TON and TOF was based on the molar amount of Ru metal in Table S1.

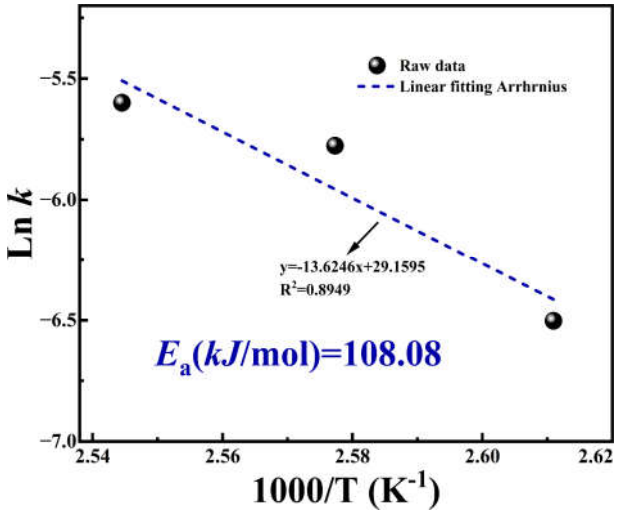

Figure S12. Arrhenius models.

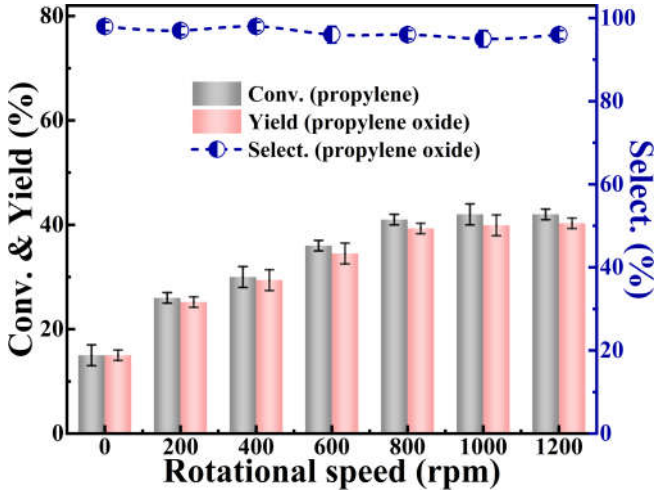

Figure S13. Performance of propylene epoxidation at different rotation speeds.

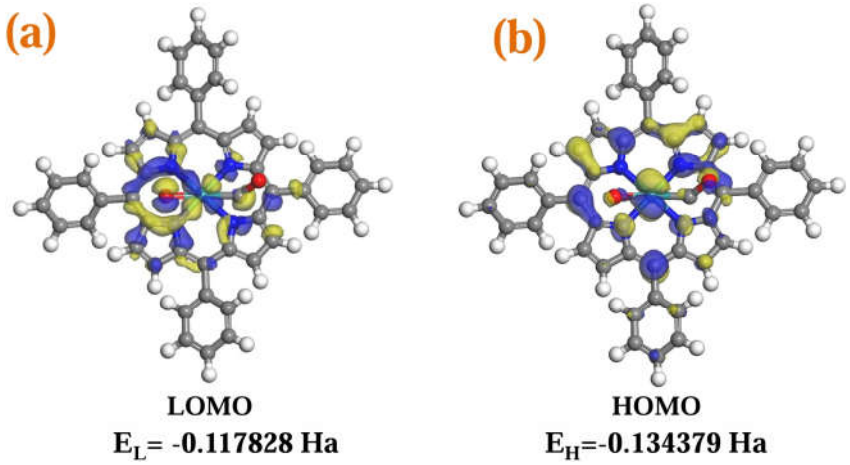

Figure S14. The molecular orbitals and energy levels for (d) LOMO and (e) HUMO of Ru=O intermediate.

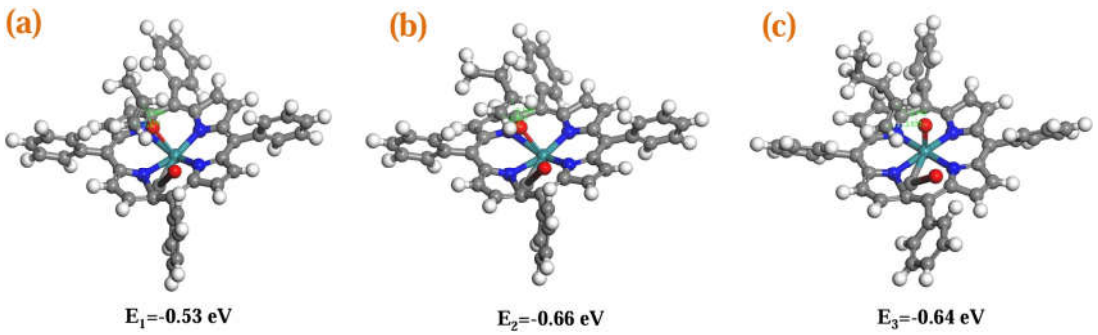

Figure S15. (a–c) The optimal geometries and binding energies of Ru=O intermediate with propylene, 1-butene, and 1-heptene, respectively.

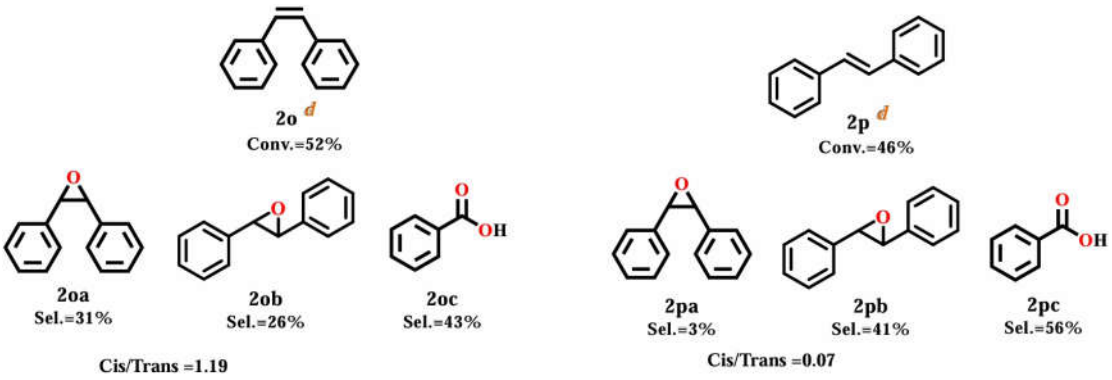

Figure S16. Product distribution of cis-stilbene and trans-stilbene.

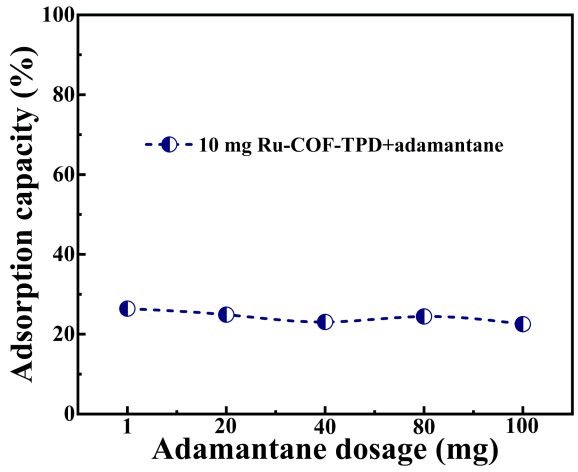

Figure S17. Adsorption experiment of adamantane (A certain amount of adamantane was added to 20 mL of acetonitrile solution containing 10 mg of catalyst. The mixture was then stirred at room temperature for 8 h, after which a sample was withdrawn for GC analysis).

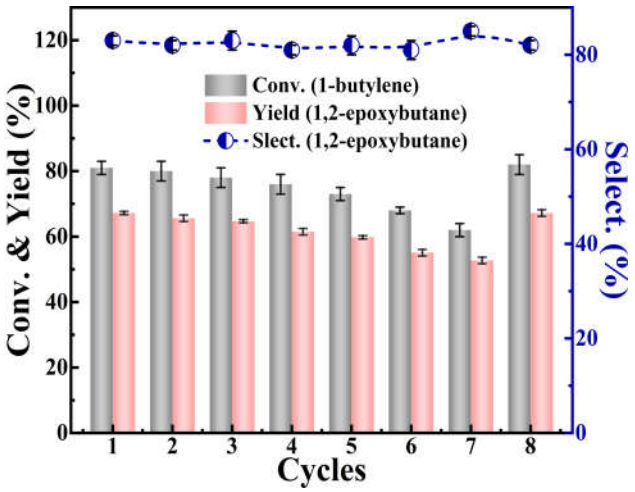

Figure S18. Reusability of the Ru-COF-TPD catalyst for 1-butylene epoxidation.

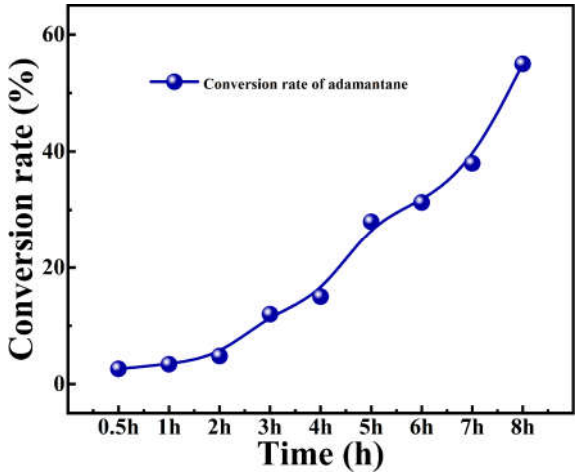

Figure S19. The conversion of adamantane at different reaction time.

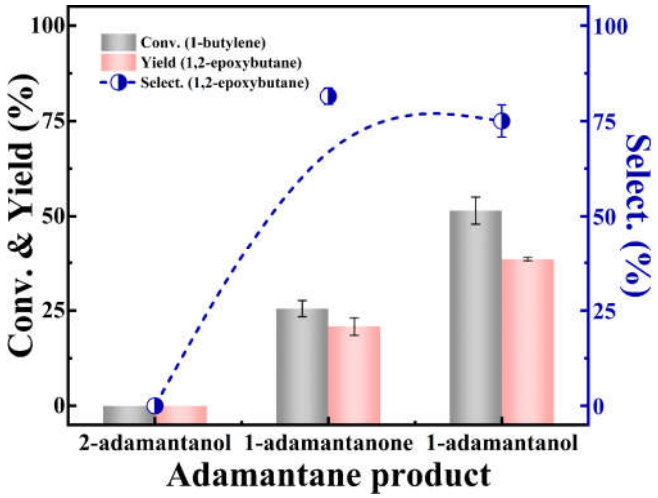

Figure S20. The performance of adamantane products.

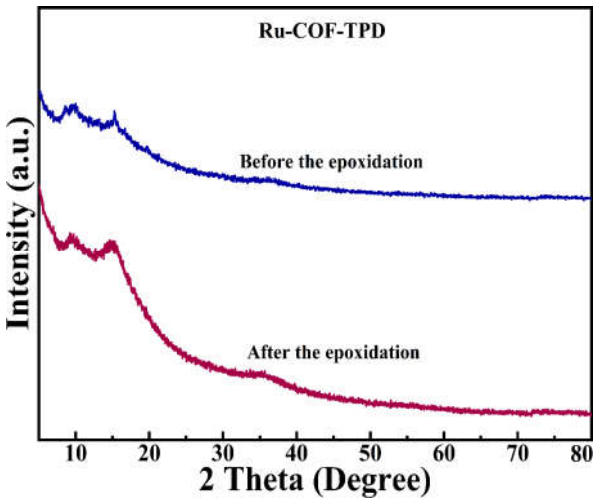

Figure S21. PXRD spectra of the catalyst before and after the reaction.

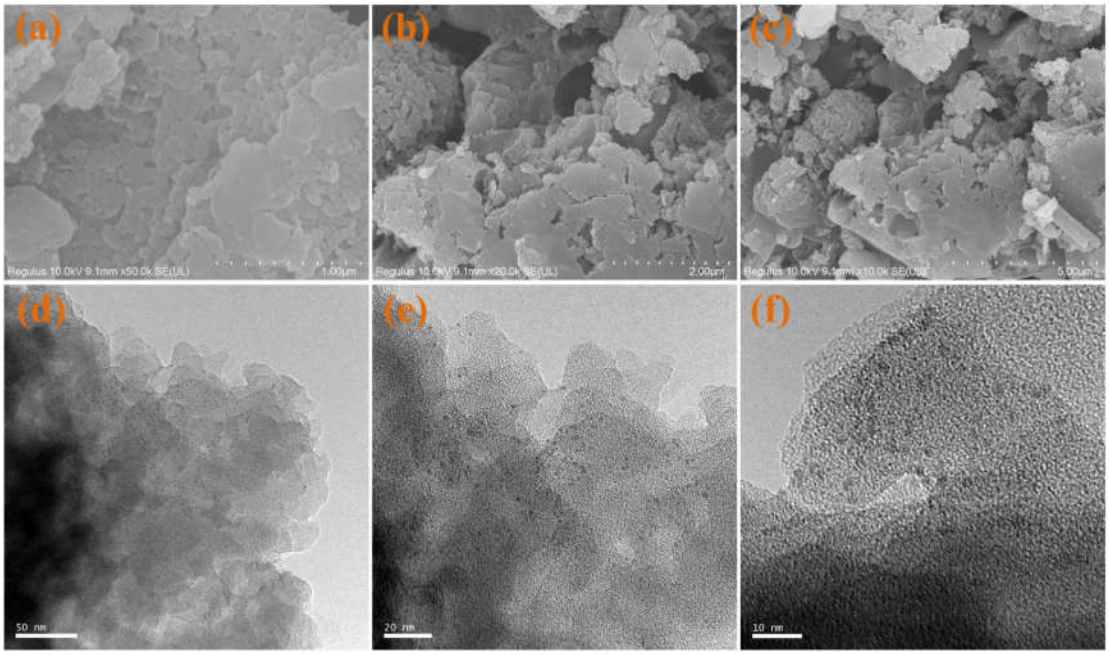

Figure S22. (a–c) SEM images of Ru-COF-TPD after the epoxidation, (d–e) TEM images of Ru-COF-TPD after the epoxidation.

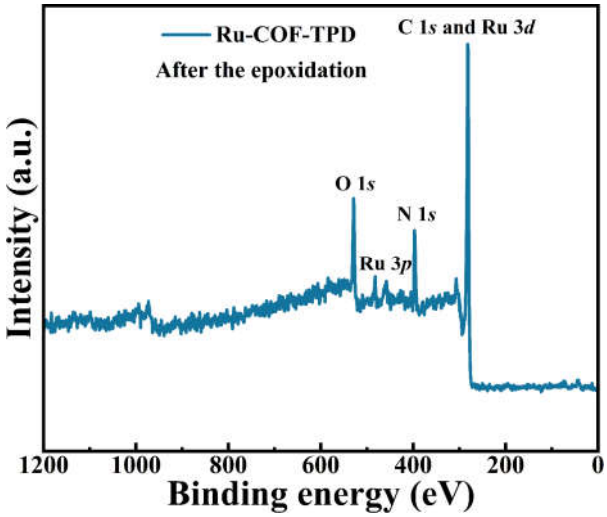

Figure S23. XPS full-scan survey spectra of Ru-COF-TPD after the epoxidation.

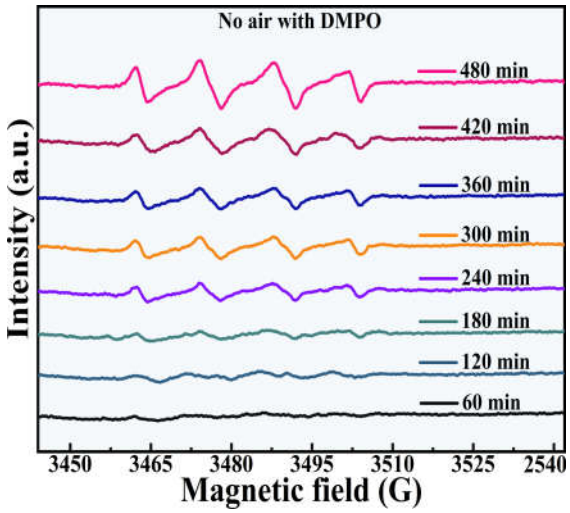

Figure S24. ESR spectra under the condition of no air at different reaction time

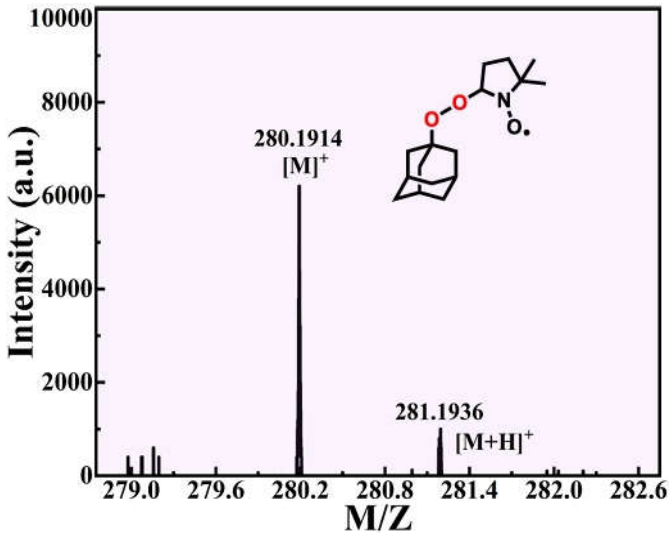

Figure S25. HRMS analysis of the peroxyl free radical.

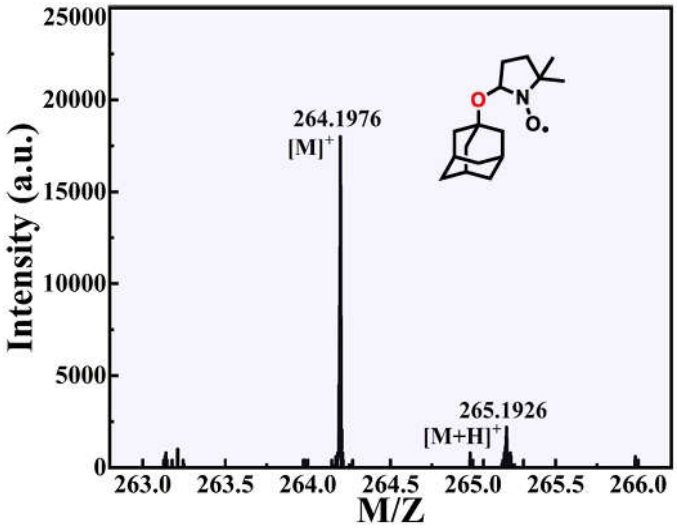

Figure S26. HRMS analysis of the alkoxyl radical.

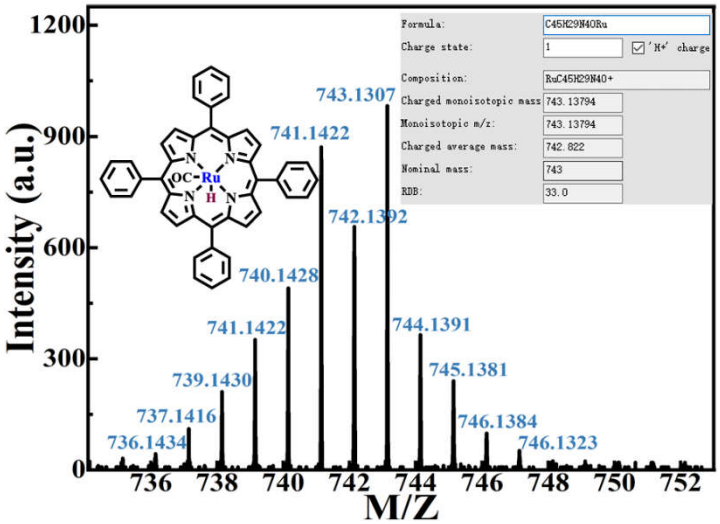

Figure S27. HRMS analysis of the Ru–H intermediate.

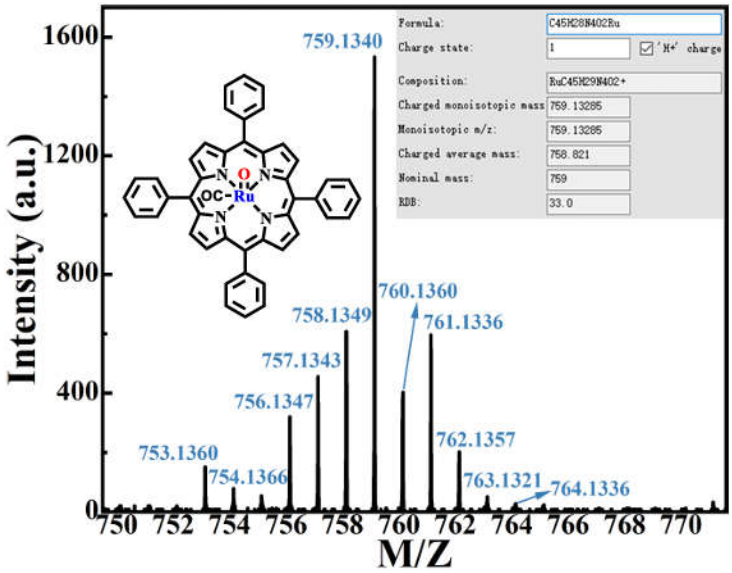

Figure S28. HRMS analysis of the Ru=O intermediate.

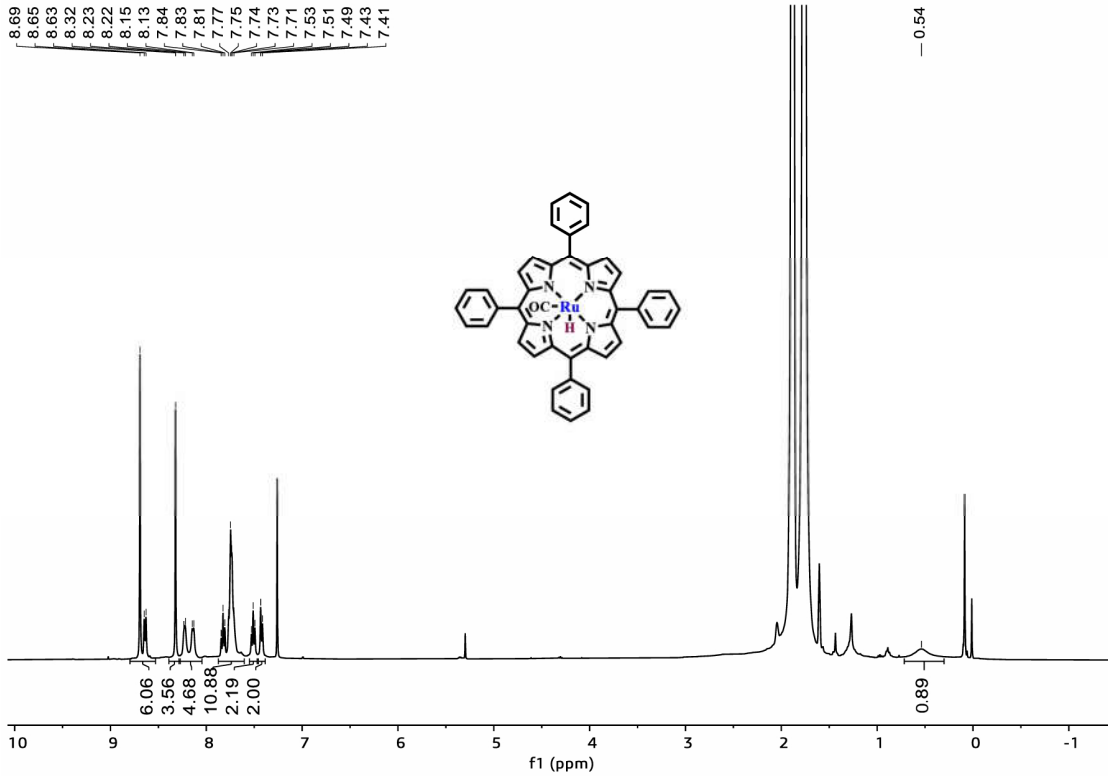

Figure S29. ^{1}H NMR (400 MHz, 20 mg of Ru-TPP and 60 mg of adamantane were dissolved 2 mL $CDCl_3$, 125 ℃, N_2, 4 h.) spectrum of Ru–H intermediate.

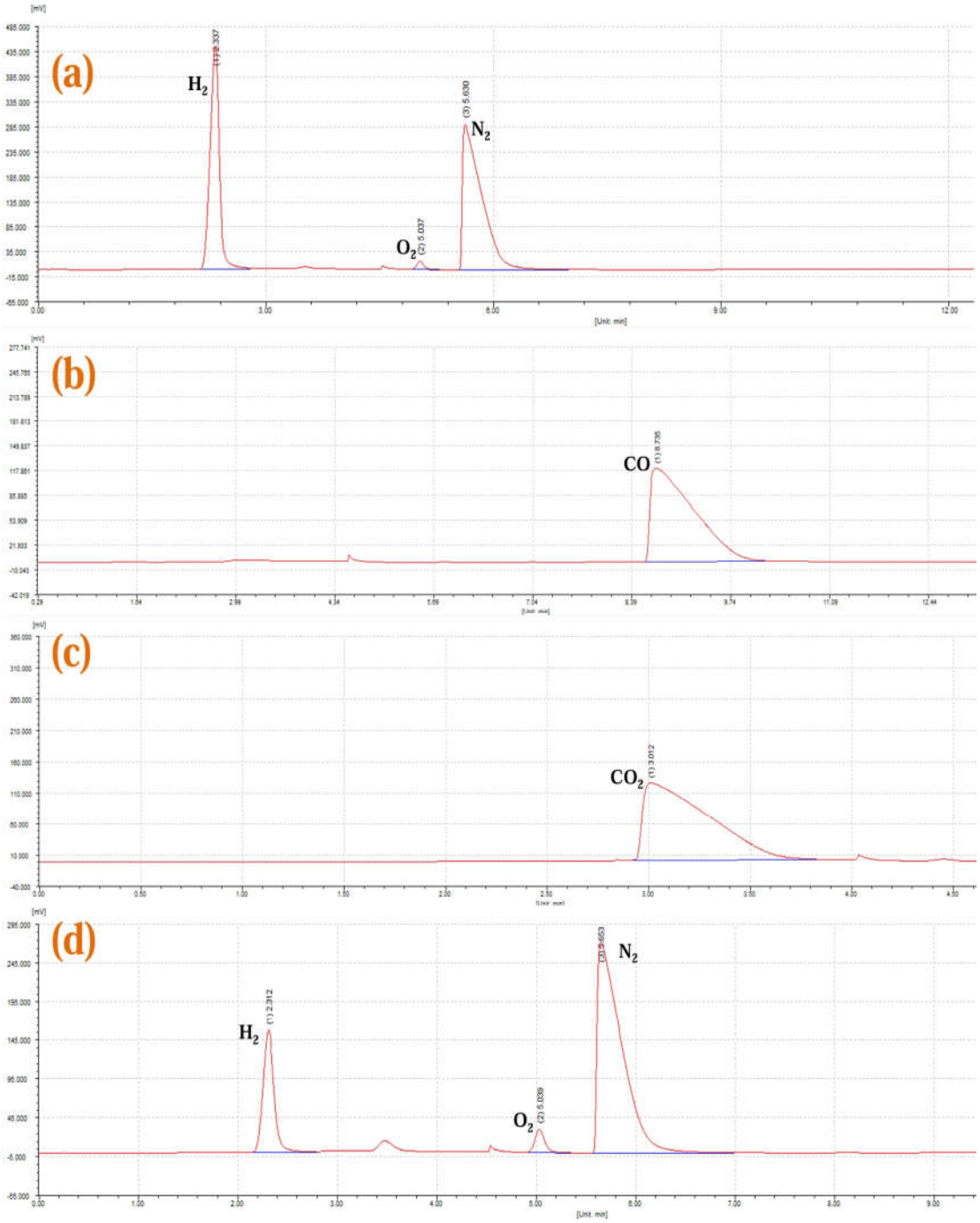

Figure S30. Chromatographic analysis: (a) standard samples of H_2, O_2 and N_2; (b) standard samples of CO, (c) standard samples of CO_2, and N_2 detection of gases after reaction. (d) detection of gases after epoxidation reaction.

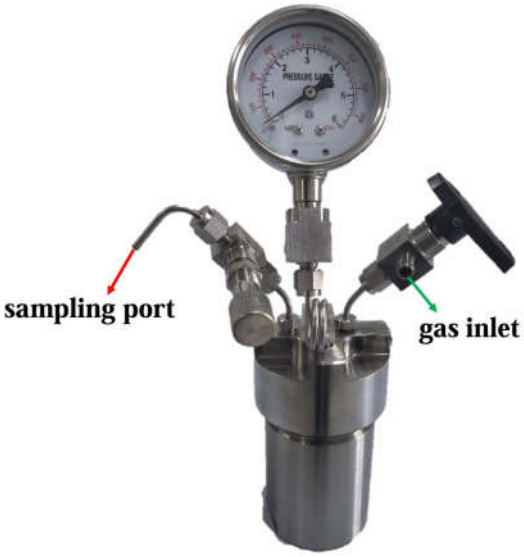

Figure S31. Reactor configuration.

Figure S32. Titration experiments: (a) the color of the catalyst in hydrochloric acid solution, (b) color after addition of xylenol orange, (c) color of the solution at the titration endpoint.

Table S1. The content of Ru metal in catalyst.

Sample	*Sampling amount (g)*	*Constant volume (mL)*	*Dilution times*	Ru content
Ru-COF-TPD before the epoxidation.	0.0479	50	400	4.82%
Ru-COF-TPD after the epoxidation.	0.0510	50	400	4.78%

Table S2. Thermodynamic parameters of 1-butylene epoxidation.

ΔS	*ΔH* (J/mol)	*T* (K)	*ΔG* (J/mol)	*Yield (EPO,%)*
856.9087	338717.3998	378	14805.9224	0.8
856.9087	338717.3998	383	10521.3790	0.8
856.9087	338717.3998	388	6236.8357	12.3
856.9087	338717.3998	393	1952.2923	27.4
−40.04164	−23111.2960	398	−7174.7244	65.9
−40.04164	−23111.2960	303	−6974.5162	61.4
−40.04164	−23111.2960	408	−6774.3080	60.4

Table S3 . Kinetic parameters of linear fitting in 1-butylene epoxidation over Ru-COF-TPD

Models	Items	Temperature (℃)		
		110	115	120
Zero order	k_0	0.0349	0.0347	0.0215
	R^2	0.7730	0.8520	0.8036
	RMSE	1.3369	1.8265	2.3635
PFO	k_1	0.0015	0.0031	0.0037
	Q_1	62.71	68.94	81.26
	R^2	0.9415	0.9775	0.9405
	RMSE	0.0416	0.0657	0.1334
PSO	k_2	0.0815	0.0201	0.0095
	Q_2	323.37	205.52	109.92
	R^2	0.3280	0.2373	0.9560
	RMSE	16.7580	5.1626	0.2506
Arrhenius	E_a (*kJ*/mol)		108.08	

Table S4. Comparison of the catalytic performances of Ru-COF-TPD and other reported for the epoxidation of 1-butylene.

Catalysts	Oxidant	t (h)	T^b (℃)	Conv. (%)	Select. (%)	Ref.
TS-1	H_2O_2	24	40	20	98	[S3]
TS-1	H_2O_2	30	45	50	90	[S4]
TS-1/SiO_2	H_2O_2	10	40	30	90	[S5]
TS-1/SiO_2/SBA-SiC	H_2O_2	10	–	30	95	[S6]
MUS	CHP	24	100	–	–	[S7]
MoOO·DMF	TBHP	1	110	40	96	[S8]
$Mo(O_2)_2$@RT	TBHP	2	110	48	92	[S9]
Cu(TBBD)	air	7	70	52	28	[S10]
Ru-COF-TPD	air	480	125	83	81	This work

3. References

[1] D. Li, C. Xiong, Q. Mao, L. Xi, T. Yang, P. Hu, H. Ji, *Nnao Res.* **2026**, 19 (1).

[2] Q. He, H. Li, Z. Hu, L. Lei, D. Wang, T. Li, *Angew. Chem. Int. Ed.* **2024**, 63 (33).

[3] M. Alvear, M. L. Reich, K. Eränen, S. Haase, D. Y. Murzin, T. Salmi, *ACS Omega.*, **2023**, 8, 25710–25726.

[4] M. Alvear, F. Orabona, K. Eränen, J. Lehtonen, S. Rautiainen, M. D. Serio, V. Russo, T. Salmi, *Chem. Eng. Sci.* **2023**, 269.

[5] T. Li, Y. Zuo, Y. Guo, H. Yang, M. Liu, X. Guo, *Catal. Sci. Technol.* **2020,** 10, 6152–6160.

[6] Y. Zuo, M. Liu, M. Ma, C. Song, X. Guo, *Ind. Eng. Chem. Res.* **2017**, 56 7462–7467.

[7] Y. Dong, J. Yuan, S. He, Z. Ma, D. Chen, C. Yang, X. Feng, *ChemCatChem* 2025, 17 (1).

[8] C. Xiong, Y. He, D. Xu, X. Liu, C. Xue, X. Zhou, H. Ji, *J. Colloid Interface Sci.* **2022**, 611, 564–577.

[9] C. Xiong, H. Liu, J. Zhou, D. Xu, Y. Liang, X. Zhou, C. Xue, H.Ji, *Nano Res.* **2023**, 16, 209–218.

[10] D. Li, C. Xiong, X. Zhao, T. Yang, Y. Wu, P. Hu, H. Ji, *J. Catal.* **2025**, 448.